Single-electron capture in 3-keV/u Ar^{8+}-He collisions

R. T. Zhang,[1] X. L. Zhu,[1] X. Y. Li,[2,3] L. Liu,[2,*] S. F. Zhang,[1] W. T. Feng,[1] D. L. Guo,[1] Y. Gao,[1] D. M. Zhao,[1] J. G. Wang,[2] and X. Ma[1,†]

[1]*Institute of Modern Physics, Chinese Academy of Sciences, Lanzhou 730000, China*

[2]*Data Center for High Energy Density Physics, Institute of Applied Physics and Computational Mathematics, Beijing 100088, China*

[3]*Hefei National Laboratory for Physical Sciences at Microscale and Department of Modern Physics University of Science and Technology of China, Heifei 230026, China*

(Received 11 November 2016; published 4 April 2017)

The electron transfer mechanism was investigated for the single-electron-capture process in 3-keV/u Ar^{8+}-He collisions with cold target recoil ion momentum spectroscopy. The different state-selective electron capture processes were identified for one $1s$ electron of He capture into $4s$, $4p$, $4d$-$4f$, and $5s$-$5p$ states of Ar^{8+}. We observed that $1s$ to $4s$ capture mainly happens at small transverse recoil ion momentum, while $1s$ to $4p$ capture mainly happens at large transverse recoil ion momentum. By comparing the measured projectile scattering angle distributions to the theoretical calculations, it is suggested that $1s$ to $4s$ and $1s$ to $4p$ state-selective capture processes are mainly caused by radial and rotational coupling effects, respectively, and the $4p_{\pm1}$ quantum states are preferred.

DOI: 10.1103/PhysRevA.95.042702

I. INTRODUCTION

Electron capture (EC) in ion-atom collisions is a process in which one electron or several electrons are transferred from the neutral atom into the charged ion. The study of EC between ions and atoms is important not only for developing fundamental scattering theory, but also for playing a vital role in many applications, for example, astrophysical and laboratory plasma formations and decay diagnostics, pumping atomic levels for recombination x-ray laser techniques, studies of biology radiation effects induced by charged ions, etc. [1,2].

From the fundamental perspective, single-electron capture (SEC) has been given much attention. It has promoted two interesting facets of atomic collisions. On the one hand, SEC gives access to energy levels of highly charged ions. These include studies with energy gain spectroscopy [3–5], photon emission spectroscopy [6–8], internal target experiment technique based on the storage ring [9–11], and cold target recoil ion momentum spectroscopy (COLTRIMS) technique [12]. On the other hand, SEC study itself is important for exploring collision dynamics and aiming at solution of few-body momentum exchange.

Based on the COLTRIMS detecting technique, numerous experimental studies on SEC differential cross sections have been carried out for intermediate-energy and high-energy collisions [13–19]. For example, Fischer *et al.* [13] have confirmed the Thomas peak with the unique projectile scattering angle $\theta = \sqrt{3}m_e/2M_p$ and concluded that the Thomas mechanism becomes the dominant contribution to the nonradiative SEC cross section at high energies. Here, m_e and M_p are the masses of the electron and the projectile, respectively. At intermediate projectile energies, electron capture occurs via an overlap of initial- and final-state wave functions that are shifted in momentum space by the projectile velocity. This is termed "velocity matching" [15,16]. These have greatly improved our understanding of the state-selective electron capture processes.

Since the first interpretation by Fano and Lichten [20], a quasimolecular promotion picture from adiabatic approximation has been extensively used in low-energy collisions [21–24]. The essence of the quasimolecular approach describing ion-atom collisions is viewed as electronic motion adiabatically adjusted to the nuclei motion of the collision partners, because the collision velocity is much smaller than the orbital velocity of the active electron. Taking the much-studied system of H^+-$He^+(1s)$ collisions, Winter *et al.* [21] have calculated the projectile scattering angle distribution by adopting $1s\sigma$ and $2p\sigma$ molecular states and $1s\sigma$, $2p\sigma$, and $2p\pi$ molecular states, respectively. It has been shown that the projectile scattering behavior is strongly dependent on the intermediate quasimolecular states. However, the experimental studies are sparse for low-energy SEC processes.

Here, SEC was investigated for 3-keV/u Ar^{8+}-He collisions. First, different state-selective electron capture into nl subshells can be resolved for the present system. Second, transfer excitations from the projectile ions and the recoil ions are found to be negligible, i.e., other electrons are frozen; this may simplify the theoretical calculations. Third, since the present projectile velocity is much smaller than the orbital velocity of the active electron, the present SEC process is a good candidate to explore the quasimolecular effects, e.g., rotational coupling and radial coupling effects, that affect the state selectivity in the SEC process.

The paper is organized as follows: The experimental method is shown in Sec. II, the off-line data analysis is explained in Sec. III, an outline of the two-center atomic orbital close coupling theory is given in Sec. IV, the results and discussion are presented in Sec. V, and the conclusions are given in Sec. VI.

II. EXPERIMENTAL METHOD

SEC between Ar^{8+} and He was performed with a COLTRIMS technique. The COLTRIMS is mounted on a

*liu_ling@iapcm.ac.cn
†x.ma@impcas.ac.cn

320-kV platform for multidisciplinary research with highly charged ions at the Institute of Modern Physics in Lanzhou, China. This high-voltage platform contains a 14.5-GHz electron cyclotron resonance ion source (ECRIS) and five experimental terminals for plasma physics, atomic physics, irradiative material, and low-energy nuclear astrophysics studies [25], of which we used the atomic physics terminal.

The principle of the COLTRIMS detecting technique has been described in Refs. [14,15,26]. Here we gave some details specific to our experiment. Ar^{8+} ions were provided by ECRIS, magnetically charge selected, and then accelerated to the desired energy. The beam line vacuum was kept to be 10^{-9} mbar so as to reduce the primary beam loss due to the collisions with residual gases. The collision chamber is more than 12 m away from the ion source. Before entering the collision chamber, the primary beam was highly collimated by two sets of slits. Typically, the beam size was about 1×1 mm^2, and the beam current was approximately 200 pA. Several sets of electrostatic deflectors were installed in front of the collision zone to steer the beam and clear out charge-state impurities from electron capture in the beam line.

A supersonic gas jet which consisted of two stages of a differential vacuum system was employed to get target atoms with higher local density. Specifically, the helium gas expanded through a 30-μm nozzle from a gas reservoir with a driving pressure of 2 bars; the gas jet was extracted through a skimmer of 0.5 mm in diameter and then entered the collision chamber. The density of the gas target was estimated to be 5×10^{11} atoms/cm^2. The ion beam intersected with a supersonic helium gas jet at a right angle in the center of the time-of-fight (TOF) spectrometer. The electrostatic field of 2.8 V/cm of TOF was used to extract the recoil ions from the collision area. The lengths of the accelerating tube and the drifting tube were 107.5 and 215 mm, which meets the Wiley-McLaren time focusing condition [27]. The charge-changed projectiles via electron capture were separated from the primary beam by an electrostatic deflector downstream of the collision chamber and detected by a position- and time-sensitive detector. This detector gave trigger signals to the clock of the data acquisition system. The primary beam was directed to a Faraday cup.

The momentum resolution of the recoil ions has been investigated in detail [28]. For the present experiment, the resolution was 0.45 a.u. The coincidence measurement between recoil ions and scattered projectile ions was applied to suppress the contamination from other processes. An event-by-event mode was employed for digital read out. By virtue of the two-dimensional spectrum containing the TOF of the recoil ions and the position of the outgoing projectile ions, the reaction channel of our greatest interest was identified and selected as follows:

$$Ar^{8+}(2p^6) + He(1s^2) \rightarrow Ar^{7+}(2p^6 nl) + He^+(1s). \quad (1)$$

Equation (1) describes the SEC, i.e., one electron of He is captured into a high-lying orbital of Ar^{8+} with the residual He^+ in the ground state. The contamination from metastable $Ar^{8+}(1s^2 2s^2 2p^5 3s)^3P_2, ^3P_0$ ions extracted from the ECR ion source is negligible due to the considerably low fraction [29].

Atomic units are used throughout this paper unless otherwise stated.

III. OFF-LINE DATA ANALYSIS

First, we defined a coordinate system with axes of x, y, and z in the laboratory frame, where the x direction was defined as the electric field direction of the TOF spectrometer, and y and z were defined as opposite of supersonic gas jet motion and beam direction, respectively.

From the hitting positions $y(i)$ and $z(i)$ on the detector plane and the time of flight $t(i)$ of each event, the momentum vectors of the recoil ion in the detector plane can be reconstructed according to the momentum definition, i.e., $P_{y,z}(i) = M_r \frac{y,z(i)}{t(i)}$, where M_r is the mass of the He^+ ion, usually a value of 7344 a.u. has been assumed. The momentum vector of the recoil ion perpendicular to the detector plane (parallel to the electric field of the TOF spectrometer) was calculated according to the formula $Px(i) = \frac{Uq}{s} \times [t_0 - t(i)]$, where q is the ionic charge, $\frac{U}{s}$ is the electric field in the TOF spectrometer, and t_0 is the time of flight of ions starting with momentum $Px = 0$. We defined the recoil ion momentum component parallel to the z direction as the longitudinal recoil ion momentum $P_{||}$, and the momentum components perpendicular to the z direction as the transverse recoil ion momentum $P_\perp$.

Especially in the approximation of the small scattering angles and the small changes of the projectile energy, the Q value of the reaction can be reflected in the longitudinal momentum of recoil ions. Thus, the longitudinal momentum of recoil ions provided directly the distribution of state-selective populations. The transverse momentum $P_\perp = \sqrt{Px^2 + Py^2}$ compensates the loss of projectile momentum in the transverse direction and provides the detailed behavior of the projectile scattering angle. The longitudinal and the transverse momentum of recoil ions can be described as the following kinematical relationship [14,15]:

$$P_{||} = -\frac{Q}{V_p} - \frac{V_p}{2}, \quad (2)$$

$$\theta = \frac{P_\perp}{P_0}, \quad (3)$$

where Q is the internal energy difference before and after the collision (total change in potential energy), V_p is the projectile velocity, P_0 is the initial projectile momentum, and θ is the scattering angle of the projectile ion.

All events originating from the SEC process were registered by the coincidence between the He^+ recoil ion and the down-charged Ar^{7+} ion. The absolute cross sections were not given due to the uncertainty of the efficiency for the recoil ion detection. The statistical error bars were simply calculated by a square root of event counts.

IV. TWO-CENTER ATOMIC ORBITAL CLOSE-COUPLING METHOD

The details of the two-center atomic orbital close-coupling method (TC-AOCC) can be found in the literature [30,31] and here only a brief account is presented. The total electron wave function of the active electron in the TC-AOCC method is expanded in terms of bound atomic orbitals of the two ionic

centers multiplied by plane-wave electron translational factors:

$$\Psi(r,t) = \sum_i a_i(t)\phi_i^A(\vec{r},t) + \sum_j b_j(t)\phi_j^B(\vec{r},t), \quad (4)$$

where the superscripts A and B designate the projectile (Ar^{8+}) and the target (He) center, respectively. The atomic states $\phi_{nlm}(r)$ are obtained as the linear combination:

$$\phi_{nlm}(\vec{r}) = \sum_k c_{nk}\chi_{klm}(\vec{r}), \quad (5)$$

where the coefficients c_{nk} are determined by diagonalization of the single-center Hamiltonian. Adopting the straight-line trajectory approximation for the relative nuclear motion $\vec{R}(t) = \vec{b} + \vec{v}t$ (b is the impact parameter and $\vec{v}$ is the collision velocity) and inserting Eq. (4) into the time-dependent Schrödinger equation $(H - \frac{i\partial}{\partial t}\Psi) = 0$, where $H = -\frac{1}{2}\nabla_r^2 + V_A(r_A) + V_B(r_B)$ and $V_{A,B}(r_{A,B})$ are the electron interaction with the target core (He^+) and the projectile (Ar^{8+}) and we represent them by model potentials, one can obtain the first-order coupled differential equations for the amplitudes $a_i(t)$ and $b_j(t)$:

$$i(\dot{A} + S\dot{B}) = HA + KB, \quad (6)$$

$$i(\dot{B} + S^\dagger\dot{A}) = \overline{K}A + \overline{H}B, \quad (7)$$

where A and B are the vectors of amplitudes $a_i(i = 1,2,\cdots,N_A)$ and $b_i(i = 1,2,\cdots,N_B)$, respectively. S is the overlap matrix ($S^\dagger$ is the transposed form), H and $\overline{H}$ are direct coupling matrices, and K and $\overline{K}$ are the electron exchange matrices. Equations (6) and (7) are solved under the initial conditions $a_i(-\infty) = \delta_{1i}$ and $b_j(-\infty) = 0$.

The angle-differential cross sections for the $i \to j$ transition can be obtained by

$$\frac{d\sigma_{ji}}{d\theta} = 2\pi\sin(\theta)|A_{ji}|^2, \quad (8)$$

where the scattering amplitudes A_{ji} are determined by the impact-parameter-dependent transition amplitudes and are given by

$$A_{ji}(\theta) = \gamma\int_0^{+\infty}\left\{bF(b)J_{|m_j-m_i|}\left[2b\mu v\sin\left(\frac{\theta}{2}\right)\right]\right\}db. \quad (9)$$

Here,

$$F(b) = a_{ji}e^{2(i/v)Z_TZ_P\ln b}, \quad (10)$$

$\gamma = \mu v(-i)^{|m_j-m_i|+1}$, μ is the reduced projectile mass, and $m_j(m_i)$ is the magnetic quantum number of the final (initial) state. The function J represents the Bessel function of the first kind and a_{ji} is the transition amplitude that is calculated from Eqs. (6) and (7) for a given impact parameter b. The $e^{2(i/v)Z_TZ_P\ln b}$ is the eikonal phase due to the Coulomb repulsion between the two nuclei and $Z_T(Z_P)$ is the effective charge of the target (projectile).

V. RESULTS AND DISCUSSION

Figure 1 shows the longitudinal recoil ion momentum for the 3-keV/u Ar^{8+}-He SEC process. It is known that the

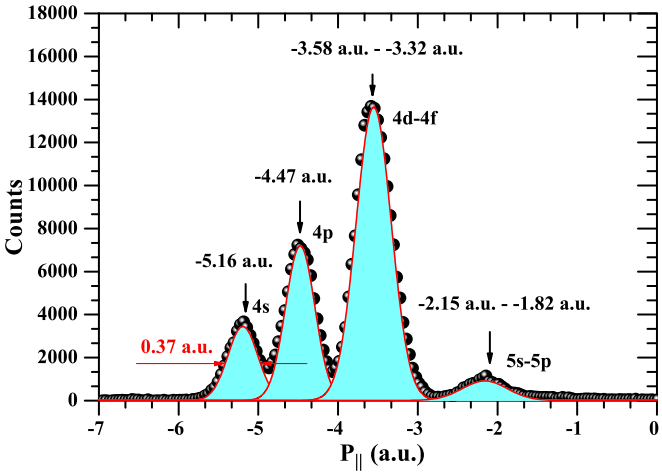

FIG. 1. The longitudinal momentum distribution of the He^+ ion. Dots represent the experimental results; red lines were obtained from multipeak Gaussian fitting.

longitudinal recoil ion momentum resolution is mainly limited by the width of the supersonic target gas jet and the gas jet density profile is approximately described by a Gaussian profile. Therefore, The Gaussian curve fitting method was adopted to extract the contribution of different state-selective capture processes. At least four peaks are resolved for $1s$ electron of He capture into $4s$, $4p$, $4d$-$4f$, and $5s$-$5p$ states of Ar^{8+}. The relative contributions of different state-selective capture were estimated to be 12.4%, 24.8%, 51.2%, and 10.1%, correspondingly.

Clearly, the state-selective capture of $n = 4$ is dominant over that of $n = 5$, this is roughly consistent with the estimation of the classical over-barrier (COB) model, i.e., the average quantum number is equal to $Z_p^{0.75}$ [32]. However, it is difficult for the COB model to predict the different states' capture involving angular momentum quantum numbers. For the capture of $n = 4$, state-selective populations were distinguished for states with angular momentum quantum numbers $l = 0$, 1, 2, and 3; these correspond to s, p, d, and f different states. The different state populations were only accessible for $l = 0$–1 for $n = 5$ capture. Due to the limitation of the experimental resolution, $4d$-$4f$ and $5s$-$5p$ capture processes can't be resolved. Additionally, it was inferred that there is a large energy level gap between $n = 3$ capture and the initial channel for the present SEC process; this results in a negligible contribution of $n = 3$ capture [33].

For $n = 4$ capture, the contribution of $4d$-$4f$ was dominant over that of $4s$ and $4p$. This is in a good agreement with the previous studies for the projectile velocity range from 0.08 to 1.0 a.u. [33–35]. From the potential curve of the molecular energy calculations, the energy level crossed with the initial channel for $4d$-$4f$ states, while the energy level did not cross with the initial channel for $4s$ and $4p$ states [33]. Nevertheless, Abdallah *et al.* [36] have suggested that dynamical coupling effects should not be ignored.

Figure 2 presents the two-dimensional momentum distribution with respect to the longitudinal and the transverse momentum of recoil ions. Clearly, the $1s$ to $4s$ capture and the $1s$ to $4p$ capture show a strong dependence on the transverse

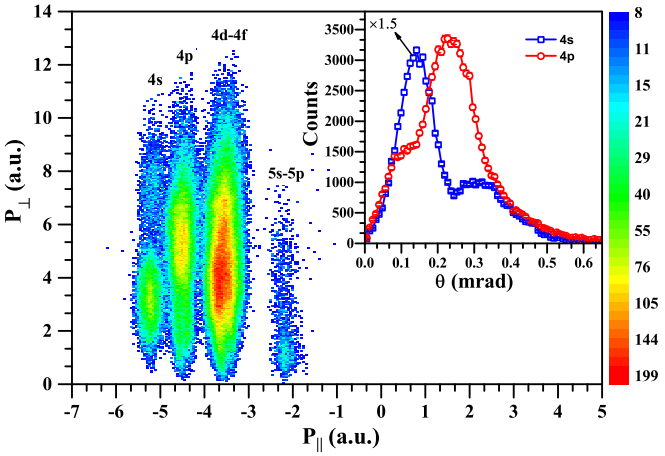

FIG. 2. Two-dimensional momentum distributions in the 3-keV/u Ar^{8+}-He SEC process. The horizontal and the vertical axes represent the longitudinal and the transverse momentum of recoil ions, respectively. In the inset plot, blue squares and red circles represent projectile scattering angle distributions for electron capture into $4s$ and $4p$ states, respectively.

recoil ion momentum distribution with the most probable values of 3 and 6 a.u., respectively. Correspondingly, the most probable values of the projectile scattering angle are 0.13 and 0.25 mrad. If the electron capture occurs due to projectile-electron interaction (so-called kinematical electron capture), the characteristic scattering angle can be estimated from $\frac{m_e}{M_p}$. For the present system, the estimated scattering angle is about 0.014 mrad. Therefore, the contribution through the kinematical electron capture mechanism can be neglected for both $1s$ to $4s$ capture and $1s$ to $4p$ capture.

To get a better understanding, differential scattering angle distributions were unfolded for the $1s$ to $4s$ and the $1s$ to $4p$ capture process, respectively. As shown in the inset figure, $1s$ to $4s$ state-selective capture mainly occurs at small projectile scattering angles (large internuclear distance), while $1s$ to $4p$ state-selective capture mainly occurs at large projectile scattering angles (small internuclear distance). This qualitatively agrees with the indication of general dynamical coupling effects, specifically radial coupling and rotational coupling effects.

Within the context of the dynamical coupling, a comparison between experimental measurements and TC-AOCC

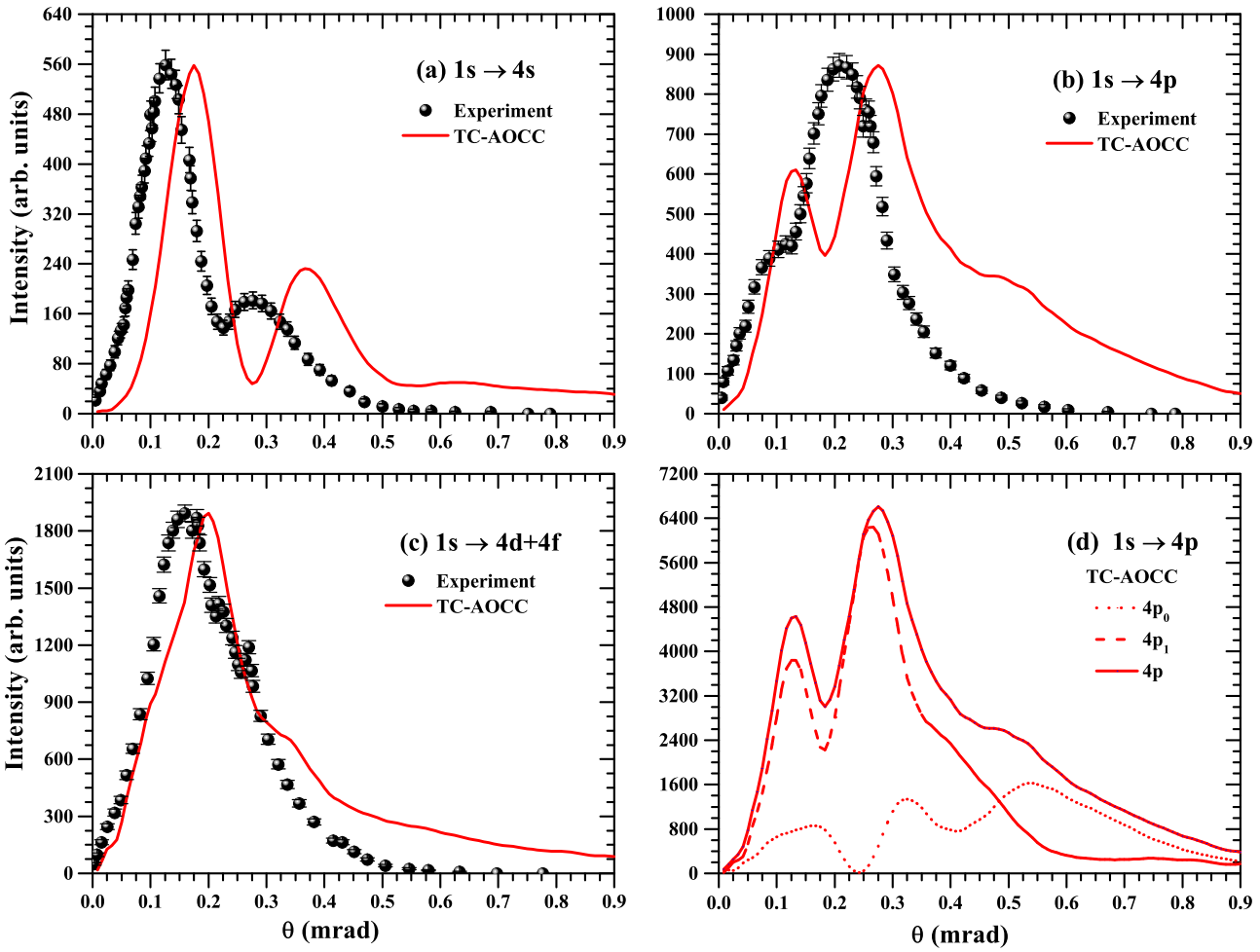

FIG. 3. Panels (a), (b), and (c) represent the comparison between experimental results and TC-AOCC theoretical calculations for $1s$ to $4s$, $1s$ to $4p$, and $1s$ to $4d+4f$ different state capture processes. Sphered represent the experimental data; the red solid line represents the theoretical calculations. Panel (d) represents the relative contribution for $1s$ to $4p_0$ and $1s$ to $4p_1$ capture. The dotted line represents electron capture into $4p_0$, the dashed line represents electron capture into $4p_1$, and the solid line is the sum of them.

calculations was performed. As shown in Fig. 3, the oscillation behaviors of the scattering angle distribution are qualitatively reproduced by the theory for $1s$ to $4s$, $1s$ to $4p$, and $1s$ to $4d$-$4f$ different state capture processes. However, the peak position of the scattering angle distribution is slightly shifted by a factor of 1.2 for $1s$ to $4s$, $1s$ to $4p$, and $1s$ to $4d$-$4f$ processes. One reason for this might be that the initial electron-electron correlation in helium is not taken into consideration for TC-AOCC calculations. There are two ways to verify this point: one is to perform lower-energy collisions and compare with the molecular orbital close coupling calculations, and the other one is to perform higher energy collisions and compare with TC-AOCC calculations directly. These will be reported in forthcoming papers.

Here, $1s$ to $4s$ and $1s$ to $4p$ capture processes are of our great interest. According to the general dynamical coupling matrix, the radial coupling can keep the projection of the angular momentum quantum number along the quantum axis (internuclear axis), while the rotational coupling can change the projection of the angular momentum quantum number along the quantum axis. Thus, it can be anticipated that the $4p_{\pm1}$ population is dominant over the $4p_0$ population. According to the TC-AOCC theoretical calculations, the relative contribution from $4p_0$ and $4p_{\pm1}$ different states is shown in Fig. 3(d). It is found that the $4p_1$ (the subscript 1 in $4p_1$ is the absolute value of ±1 in $4p_{\pm1}$ unless it is stated otherwise) state is more preferentially populated than the $4p_0$ state. This indicates that the $4p$ state is strongly aligned and the information of the magnetic quantum number is well distinguished for the present capture process.

In future experiments, we will aim at improving the longitudinal momentum resolution to better than 0.1 a.u. A better resolution would allow us to resolve the population for different states, which is not available in the present study. Furthermore, the alignment effects of the electron cloud (e.g., the d and f electrons) can be examined for the SEC process in slow highly charged ion-atom collisions.

VI. CONCLUSIONS

We have investigated the electron transfer mechanism for the SEC process in 3-keV/u Ar^{8+} on He collisions. By measuring the longitudinal momenta of recoil ions, different state-selective electron capture processes were identified for one $1s$ electron capture into $4s$, $4p$, $4d$-$4f$, and $5s$-$5p$ of Ar^{8+}. It is found that the contribution of $1s$ to $4d$-$4f$ capture is dominant and the contributions of $1s$ to $4s$, $1s$ to $4p$, and $1s$ to $5s$-$5p$ are minor. Furthermore, by unfolding the scattering angle distributions, we observed that $1s$ to $4s$ capture mainly happened at small transverse recoil ion momentum (large internuclear distance), while $1s$ to $4p$ transition mainly happened at large transverse recoil ion momentum (small internuclear distance). Compared to the theoretical calculations, it is concluded that the $1s$ to $4s$ and $1s$ to $4p$ state-selective electron capture processes are mainly caused by the radial and the rotational couplings which probably drive the intermediate quasimolecular states' transition, and the resulting $4p_{\pm1}$ quantum states are preferred.

ACKNOWLEDGMENTS

X.L.Zh and L.L were supported by the National Natural Science Foundation of China under Grants No. 11274317 and No. 11474033, respectively. R.T.Zh. acknowledges the support provided by the China Postdoctoral Science Foundation (Grant No. 2015M582729). Many thanks are given to the engineers who operated the 320-kV platform for their assistance in running the ECR ion source.

[1] B. H. Bransden and M. R. C. McDowell, *Charge Exchange and the Theory of Ion-Atom Collisions* (Oxford University, London, 1992).

[2] H. S. W. Massey, E. W. McDaniel, and B. Bederson, *Applied Atomic Collision Physics Vol 1* (Academic, San Diego, 1982).

[3] K. Okuno, H. Tawara, T. Iwai, Y. Kaneko, M. Kimura, N. Kobayashi, A. Matsumoto, S. Ohtani, S. Takagi, and S. Tsurubuchi, Phys. Rev. A **28**, 127 (1983).

[4] C. Schmeissner, C. L. Cocke, R. Mann, and W. Meyerhof, Phys. Rev. A **30**, 1661 (1984).

[5] B. A. Huber and H. J. Kahlert, J. Phys. B: At. Mol. Phys. **16**, 4655 (1983).

[6] S. Bliman, R. Bruch, M. Cornille, A. Langereis, and J. Nordgren, Phys. Rev. A **66**, 052707 (2002).

[7] T. Hayakawa, R. A. Lomsadze, C. Verzani, H. Watanabe, H. Tanuma, B. D. DePaola, and N. Kobayashi, Phys. Scr. **T92**, 322 (2001).

[8] A. Kivimäki, A. Naves de Brito, S. Aksela, H. Aksela, O.-P. Sairanen, A. Ausmees, S. J. Osborne, L. B. Dantas, and S. Svensson, Phys. Rev. Lett. **71**, 4307 (1993).

[9] J. Eichler and T. Stöhlker, Phys. Rep **439**, 1 (2007).

[10] M. Trassinelli, C. Prigent, E. Lamour, F. Mézdari, J. J. Mérot, R. Reuschl, J. P. Rozet, S. Steydli, and D. Vernhet, J. Phys. B: At. Mol. Phys. **45**, 085202 (2012).

[11] G. Bednarz, A. Warczak, D. Sierpowski, T. Stöhlker, S. Hagmann, F. Bosch, A. Gumberidze, C. Kozhuharov, D. Liesen, P. H. Mokler *et al.*, Nucl. Instrum. Methods Phys. Res., Sect. B **235**, 280 (2005).

[12] J. Ullrich and V. Shevelko, *Many-Particle Quantum Dynamics in Atom and Molecular Fragmentation* (Springer, New York, 2003).

[13] D. Fischer, M. Gudmundsson, Z. Berényi, N. Haag, H. A. B. Johansson, D. Misra, P. Reinhed, A. Källberg, A. Simonsson, K. Støchkel *et al.*, Phys. Rev. A **81**, 012714 (2010).

[14] J. Ullrich, R. Moshammer, A. Dorn, R. Dörner, L. P. H. Schmidt, and H. Schmidt-Böcking, Rep. Prog. Phys. **66**, 1463 (2003).

[15] R. Dörner, V. Mergel, O. Jagutzki, L. Spielberger, J. Ullrich, R. Moshammer, and H. Schmidt-Böcking, Phys. Rep. **330**, 95 (2000).

[16] M. A. Abdallah, W. Wolff, H. E. Wolf, E. Y. Kamber, M. Stöckli, and C. L. Cocke, Phys. Rev. A **58**, 2911 (1998).

[17] V. Mergel, R. Dörner, J. Ullrich, O. Jagutzki, S. Lencinas, S. Nüttgens, L. Spielberger, M. Unverzagt, C. L. Cocke, R. E. Olson *et al.*, Phys. Rev. Lett **74**, 2200 (1995).

[18] H.-K. Kim, M. S. Schöffler, S. Houamer, O. Chuluunbaatar, J. N. Titze, L. P. H. Schmidt, T. Jahnke, H. Schmidt-Böcking, A. Galstyan, Y. V. Popov *et al.*, Phys. Rev. A **85**, 022707 (2012).

[19] R. Dörner, J. Ullrich, H. Schmidt-Böcking, and R. E. Olson, Phys. Rev. Lett **63**, 147 (1989).
[20] U. Fano and W. Lichten, Phys. Rev. Lett. **14**, 627 (1965).
[21] T. G. Winter, G. J. Hatton, and N. F. Lane, Phys. Rev. A **22**, 930 (1980).
[22] W. Fritsch, J. Phys. B: At. Mol. Phys. **27**, 3461 (1994).
[23] E. J. Shipsey, T. A. Green, and J. C. Browne, Phys. Rev. A **27**, 821 (1983).
[24] C. H. Liu, L. Liu, and J. G. Wang, Phys. Rev. A **90**, 012708 (2014).
[25] X. Ma, H. P. Liu, L. T. Sun, M. T. Song, X. L. Zhu, S. Sha, W. T. Feng, D. C. Zhang, S. F. Zhang, B. Li *et al.*, J. Phys: Conf. Ser. **163**, 012104 (2009).
[26] X. Ma, R. T. Zhang, S. F. Zhang, X. L. Zhu, W. T. Feng, D. L. Guo, B. Li, H. P. Liu, C. Y. Li, J. G. Wang *et al.*, Phys. Rev. A **83**, 052707 (2011).
[27] W. C. Wiley and I. H. McLaren, Rev. Sci. Instrum. **26**, 1150 (1955).
[28] D. L. Guo, X. Ma, W. T. Feng, S. F. Zhang, and X. L. Zhu, Acta Phys. Sin. **60**, 113401 (2011).
[29] P. Boduch, M. Chantepie, D. Hennecart, X. Husson, H. Kucal, D. Lecler, and N. Stolterfoht, Phys. Scr. **45**, 203 (1992).
[30] L. Liu, C. H. Liu, J. G. Wang, and R. K. Janev, Phys. Rev. A **84**, 032710 (2011).
[31] L. Liu, J. G. Wang, and R. K. Janev, Phys. Rev. A **83**, 012712 (2011).
[32] V. G. Pal'chikov and V. P. Shevelko, *Reference Data on Multicharged Ions* (Springer, New York, 1995).
[33] M. Druetta, S. Martin, T. Bouchama, C. Harel, and H. Jouin, Phys. Rev. A **36**, 3071 (1987).
[34] M. Kimura and R. E. Olson, Phys. Rev. A **31**, 489 (1985).
[35] A. Bordenave-Montesquieu, P. Benoit-Cattin, M. Boudjema, A. Gleizes, and S. Dousson, Nucl. Instrum. Methods Phys. Res., Sect. B **23**, 94 (1987).
[36] M. A. Abdallah, W. Wolff, H. E. Wolf, E. Sidky, E. Y. Kamber, M. Stöckli, C. D. Lin, and C. L. Cocke, Phys. Rev. A **57**, 4373 (1998).